Monoenergetic Positronium Emission from Metal-Organic Framework Crystals

A. C. L. Jones, H. J. Goldman, Q. Zhai, P. Feng, H. W. K. Tom, and A. P. Mills, Jr.

Phys. Rev. Lett. **114**, 153201 — Published 17 April 2015

DOI: 10.1103/PhysRevLett.114.153201

Monoenergetic positronium emission from metal-organic framework (MOF) crystals

A. C. L. Jones[1],* H. J. Goldman[1], Q. Zhai[2], P. Feng[2], H. W. K. Tom[1], and A. P. Mills, Jr.[1]
[1] *Department of Physics and Astronomy, University of California, Riverside, CA 92521 and*
[2] *Materials Science and Engineering Program and Department of Chemistry, University of California, Riverside, CA 92521*
(Dated: March 9, 2015)

Recently it has been discovered that positronium (Ps), after forming in metal-organic framework (MOF) crystals, is emitted into vacuum with a high efficiency and low energy that can only be explained by its propagating as delocalized Bloch states. We show that the Ps atoms are emitted from MOFs in a series of narrow energy peaks consistent with Ps at Bloch-state energy minima being emitted adiabatically into the vacuum. This implies that the Ps emission energy spectra can be directly compared with calculations to obtain detailed information about the Ps band structure in the MOF crystal. The narrow energy width of the lowest energy Ps peak from one MOF sample (ZIF-8) suggests it originates from a polaronic Ps surface state. Other peaks can be assigned to Ps with an effective mass of about twice that of bare Ps. Given the immense catalog of available MOF crystals, it should be possible to tune the Ps properties to make vastly improved sources with high production efficiency and a narrow energy spread, for use in fundamental physics experiments.

Metal-organic frameworks are a class of materials composed of metal-based nodes, with organic linkers forming highly ordered, porous, crystalline structures, and are available with an enormous variety of compositions and structures. These properties have made MOFs promising candidate materials for H_2 storage, catalytic reactions, and chemical separation, particularly since a class of stable MOF structures were first synthesized in 1999 [1]. It is these same properties that make MOFs promising targets for the production, manipulation, and study of the electron-positron atom positronium (Ps) [2–4]. In MOF crystals, Ps will exist in Bloch states [5], provided that it does not become trapped in local lattice imperfections. To corroborate the first experimental evidence for Ps Bloch states in MOF materials [6], Crivelli and coworkers [7] made measurements of the energies of Ps emitted from MOF surfaces by time-of-flight (TOF) spectroscopy, which measures the surface-normal components of the Ps velocities. The observation that Ps was emitted with kinetic energies much smaller than would be anticipated for Ps confined within individual MOF unit cells was taken as evidence confirming that the Ps exists in Bloch states. However, due to the wide angular acceptance of the apparatus, narrow energy features associated with Ps in Bloch states with low crystal momentum k, which should be present for thermalised Ps, could not be directly observed. Using angle-resolved Ps emission energy spectroscopy, we are able to resolve narrow energy peaks associated with the Ps Bloch states posited by Dutta *et al.* [6], thus providing insight into the dynamics of Ps interacting with the MOF crystals.

The experiments reported here achieve high resolution by converting ground state ortho-Ps (142 ns mean lifetime) into long-lived ($\sim 30\mu$s [8]) Rydberg states [9]. The Ps kinetic energies are then found with high accuracy from their flight times over distances that are substantially longer than otherwise possible using ground-state Ps. A ^{22}Na source and solid Ne moderator [10] are used to load a buffer gas trap [11] which produces 10 ns bursts of $\sim 10^5$ positrons every 4.4 s. The positrons are guided by a (21 ± 1) mT axial magnetic field and implanted into a Ps-forming target after acceleration to kinetic energies up to 5.2 keV using a pulsed electrode.

The targets are powdered MOF samples, ZIF-8 (2-Methylimidazole zinc salt from Sigma-Aldrich) and MOF-5 (1,4-benzenedicarboxylate zinc salt prepared by Q. Zhai) [1], lightly pressed onto a strip of double-sided carbon adhesive tape mounted on a strip of Ta in thermal contact with a 10 K closed-cycle refrigerator. Long-lived Rydberg atoms are detected at a microchannel plate (MCP) in a cone of half angle 1.35° normal to the target surface, after a flight path of $L = (1.78 \pm 0.01)$ m. The flight times, 3 to 10 μs for 1 to 0.1 eV Ps, are determined with an overall uncertainty of $\pm$ 10 ns. The energy uncertainties thus range from $\pm$ 9 meV at 1 eV to $\pm$ 0.6 meV at 0.1 eV, including the uncertainty in the flight path. When combined with the narrow angular resolution, this results in at least an order of magnitude improvement in the energy resolution of TOF measurements performed using ground state Ps atoms (*e.g.*, [12]).

Ps emitted from the target was optically excited into Stark-split Rydberg states via a two-step process [$1S$-$2P \rightarrow n = 30 \pm 1$] using a pair of pulsed dye lasers generating visible light at 486 nm, which is subsequently doubled to 243 nm, and IR light at 732 nm. At the end of their flight path, the Rydberg Ps atoms are field-ionized in the $\sim$ 1.5 kV/cm electric field produced by a pair of 85 mm diameter grids with a 3 mm separation. The ionized positrons are accelerated and focused onto a 4 cm diameter MCP detector. Each event signaling the detection of a Rydberg Ps atom is recorded as a wavelength and TOF pair (λ, t), with the IR wavelength λ measured at a Bristol 821 pulsed wavelength meter [13]. The start time is determined from the MCP signal due to annihilation photons at the target with the lasers off. The data are saved as a list of event times rounded to the nearest

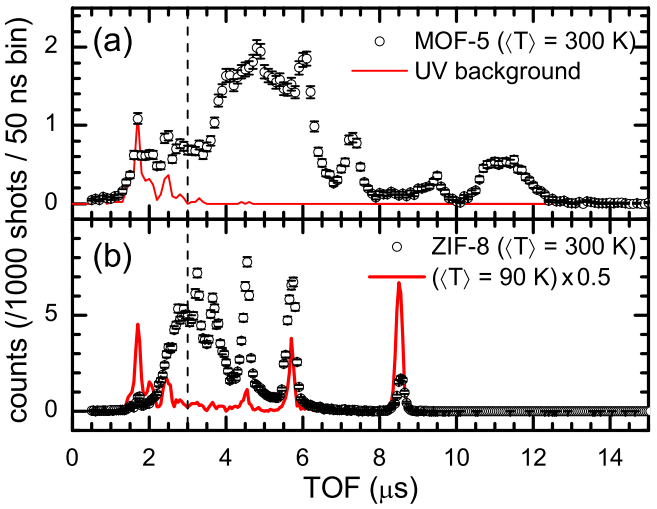

FIG. 1. (color online) TOF spectra for Ps emission from the MOF crystals (a) MOF-5 and (b) ZIF-8. Spectra shown are the sum of scans taken with positron implantation energies in the range 0.2-5.2 keV, with the targets at room temperature (open circles, 300 K), and for ZIF-8 at low temperature (bold line, 90 K). Also shown in plot (a) is a background spectrum (solid line), resulting from ions generated in the detector due to scattered UV light, scaled to the first peak in the spectrum of MOF-5. The observed background is negligible for flight times greater than 3 μs (indicated by the dashed vertical line), corresponding to Ps kinetic energies $\geq$ 2 eV and has not been subtracted from the data.

5 ns interval.

In Fig. 1 the count rate as a function of TOF is presented for positrons implanted into the MOF-5 and ZIF-8 targets, summed from scans taken with positron kinetic energies K between 0.2 to 5.2 keV. The spectra consist of broad, non-thermal distributions of counts upon which are superimposed a number of distinct peaks. For flight times less than $\sim$ 3 μs, there is a background signal due to ions generated in the detector from scattered UV light, appearing as a series of peaks, shown in Fig. 1 (a). The data are summed into equal-width energy bins to yield energy distributions, as shown in Fig. 2 (a) and (b) for MOF-5 and ZIF-8 samples at both room ($\sim$ 300 K) and cryogenic temperatures ($\langle$T$\rangle$ = 115 and 80 K, respectively). The most prominent energy peaks of MOF-5 and ZIF-8 are labeled E1-E4.

Although not shown in the figures, as the positron energy is increased from 0.2 to 5.2 keV, the MOF-5 E1 peak increases from 20% to 60% of the total, the E2 peak grows from 6% to 12% and the E3 and E4 peaks diminish. This behavior is explained as follows: Positronium with energies from 0 to a few eV is formed a few ps after positrons of kinetic energy K are implanted into the sample. The Ps then diffuses towards the sample surface, while losing energy to phonons and consequently shifting its population to lower and lower energy Bloch states and accumulating intensity near the Bloch state minima due to the energy gaps, as illustrated in Fig. 2 (c). While near the surface, Ps atoms in Bloch states that couple to states of Ps in the vacuum are emitted, typically leaving the sample in its ground state. Since the time spent in the sample increases with implantation depth and hence K, we expect the lowest energy emission peak E1, which would correspond to the lowest energy Bloch-state minimum in the solid, to increase in amplitude with K. The higher energy peaks E3 and E4 are diminishing and the E2 peak, being fed by E3 and E4 and depleted to E1, appears to maintain a roughly constant intensity for $1 < K < 5$ keV.

It thus appears that the peaks E1-E4 from MOF-5 may be ascribed to adiabatic Ps emission into the vacuum from Bloch-state minima. The same picture does not appear to be valid for ZIF-8 data where the intensities of the E1 and E2 peaks are constant for $2 < K < 5$ keV, having initially increased for $0.2 < K < 2$ keV at the expense of the E3 peak. It appears that the state responsible for the E1 peak is not being populated during the time the Ps corresponding to the E2 peak is diffusing towards the surface, otherwise peak E1 would increase and E2 would decrease as K gets larger. We conclude that the state E1 is being populated after the E2 Ps atoms reach the surface, and that the E1 peak is due to Ps emission from a metastable surface state. The narrowness of the E1 peak would then be due to the E1 surface state being localized or having a large effective mass ($m^*_{\rm Ps}$). The existence of a surface Ps state is not unreasonable given the evidence for such a state on a dielectric crystal, *i.e.*, quartz single crystals [14].

Examination of plots (a) and (b) of Fig. 2 reveals that peaks E2 and E3 for both samples have similar shapes $N(E)$, with a sharp step-like feature on the low energy side and an exponential decay on the high energy side. On the other hand the E1 peaks, although narrow, do not have this shape. We examine these peaks for ZIF-8 in detail in Fig. 3. As illustrated in Fig. 2 (c), Ps will accumulate near the bottom of any energy bands which have relatively low rates of transition to lower bands, *e.g.*, E2 and E3. The spectrum of adiabatically emitted Ps energies E from a parabolic band minimum will be a beam-Maxwellian displaced by the Ps negative affinity A for the level in question,

$$\frac{dN(E)}{dE} = \Theta(E-A)(E-A)e^{\left(\frac{-(E-A)}{k_B T}\right)}. \qquad (1)$$

The shape described by the above distribution fits peaks E2 and E3 for both MOF-5 and ZIF-8, as illustrated in Fig. 3 for ZIF-8. We notice, however, that there is a tail to lower energies from these peaks, which might represent inelastic emission, *i.e.*, one or more phonons have been shaken off during the emission process.

This same description does not apply to the two E1 peaks. The shape of the MOF-5 E1 peak is explained as being due to the otherwise parabolic band being flattened

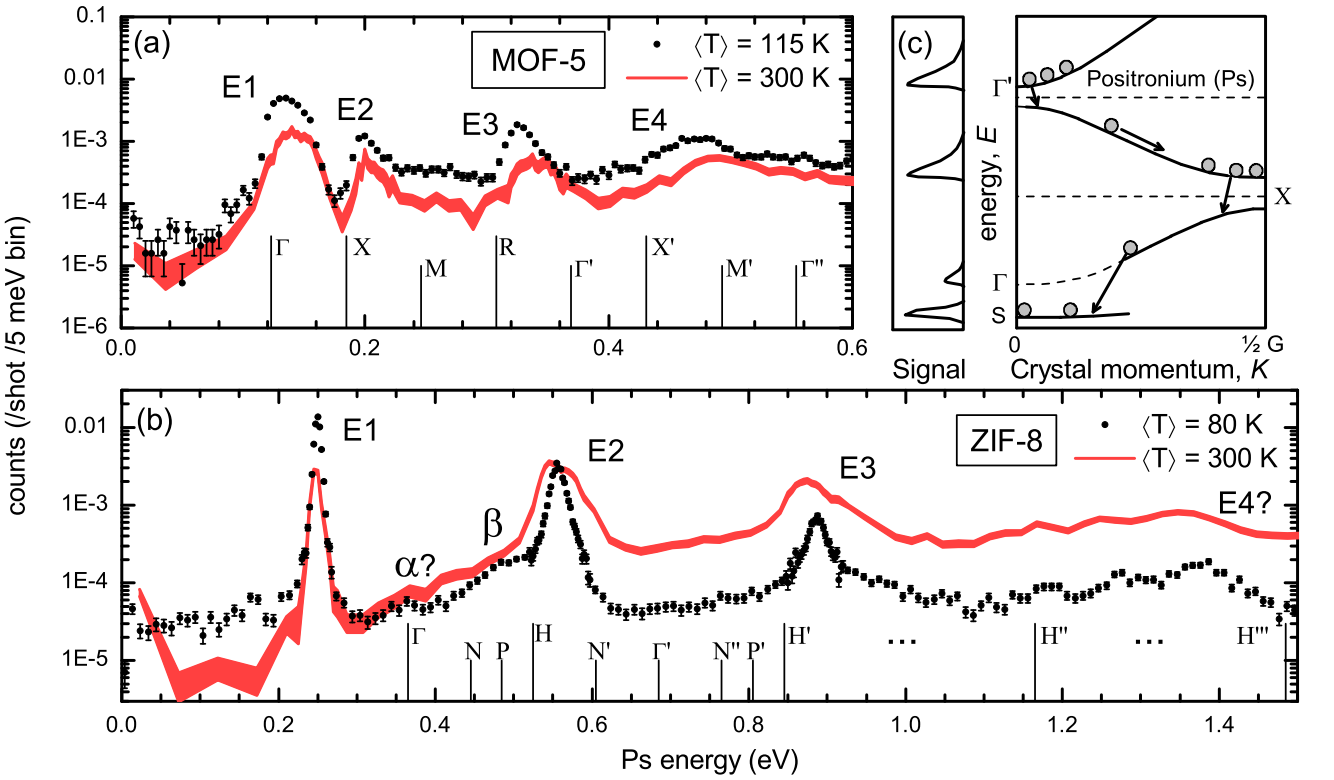

FIG. 2. (color online) Kinetic energy spectra for Ps emitted from the MOF crystals (a) MOF-5 and (b) ZIF-8, taken with the target at room temperature (band) and cryogenic temperatures (filled circles). The statistical uncertainty is represented by errorbars in the low temperature data, and by the width of the filled band for the room temperature data. The most prominent peaks are labelled E1 - E4. Tentative band assignments are shown at the bottom of each plot. In the ZIF-8 spectrum, two additional features are indicated, labelled α and β. (c) A representation of the model of the observed Ps emission spectra from MOF targets. Ps thermalising in the target cascades between Ps Bloch states, collecting in band minima. The lowest energy state of ZIF-8, labelled S, is not observed for MOF-5, but may exist and be too tightly bound to emit Ps.

by the first energy gap, *i.e.*, the band range $E(\Gamma \to X)$ of Fig. 2 (c) $\sim k_B T$. The ZIF-8 E1 peak, on the other hand, is fitted by a Gaussian having a standard deviation of about 4 meV at both 90 K and 300 K, a factor of 2-6 less than what would be expected if the width were associated with sample temperatures. This finding is in agreement with our assignment of the E1 peak of ZIF-8 as originating from a surface Ps state (see band S of Fig. 2 (c)).

We now attempt to identify the band gap minima that correspond to the Ps emission peaks. We start with the empty lattice energy bands for simple cubic MOF-5 and body centered cubic ZIF-8. We assume the appropriate lattice constant for MOF-5 is $a = 1.29$ nm because the band gaps associated with the full unit cell of 2.58 nm are probably very small [7]. The empty lattice band gap centers will thus be at various integral multiples n of energies

$$E = n\frac{\pi^2\hbar^2}{2m^*_{\rm Ps}a^2} = n \times (113\ {\rm meV}/M^*), \qquad (2)$$

where $M^* = m^*_{\rm Ps}/(2m_e)$ is the relative Ps effective mass due to its being dressed with virtual phonons in the sample [15]. Taking the lowest energy at the Γ point ($k = 0$) to be the fitted zero of the E1 peak, 123 meV, the choice of $M^* = 1.85$ results in the empty lattice energy for point X on the Brillouin zone being located 30 meV below peak E2. The peak E3 is then associated with the R point and E4 with the X′ point. The absence of observed peaks at energies corresponding to the intervening M and Γ′ points can be explained by assuming either that the band gaps are so small that no significant amount of Ps lingers there, or that there is no significant coupling of such states to vacuum Ps states.

The empty band gaps of ZIF-8 are spaced by various integral multiples of energies $E = n \times (65\ {\rm meV}/M^*)$. One can assign peaks E2 and E3 to the energy minima above the empty lattice band gaps at symmetry points H and H′ using $M^* = 1.63$, assuming Γ, N, and P do not have metastable minima and that the lowest energy Γ Ps cannot be populated. Otherwise E2 would have to correspond to the lowest energy Bloch state, and the peak E3 to H with $M^* = 1$. A possible small amplitude peak α at 365 meV could be the Γ point, which would

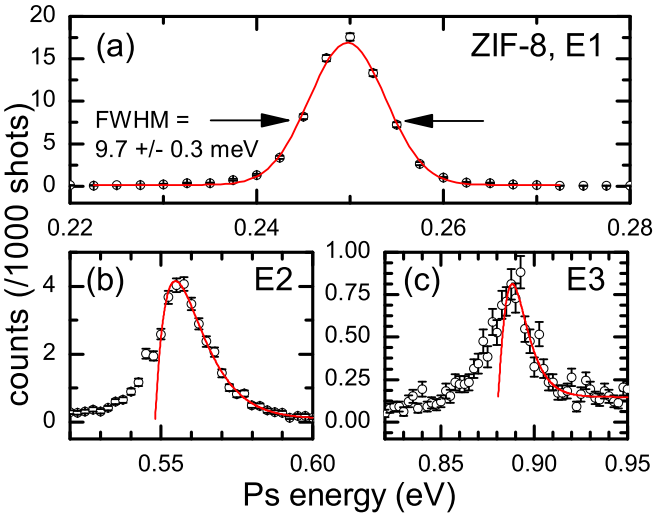

FIG. 3. (color online) Plots (a)-(c) display peaks E1-E3 from the composite spectrum of Ps emission energy from 80 K ZIF-8. In plot (a) the lowest energy peak, E1, is shown along with a gaussian fit, indicating a sub-thermal energy width of 9.7 ± 0.3 meV. Plots (b) and (c) show peaks E2 and E3, and a fitted Beam-Maxwellian, which yield temperatures consistent with the target temperature.

then have to not be easily reachable from the Bloch state corresponding to E2. A broad peak β at 480 meV could be associated with point P on the Brillouin zone, or with nonadiabatic emission associated with the E2 peak due to shake-off of ~ 50 meV longitudinal optical phonons. As for the lowest energy peak (E1), the fact that it is very close to monoenergetic implies not only a very narrow energy band due to a polaronic state [15–18], but also that the phonon cloud around the Ps collapses adiabatically as the Ps is emitted into the vacuum. Nonadiabatic emission events do appear, forming a tail at energies below the peak, and account for $\sim 1\%$ of the events in the narrow peak.

Our experiments and those of Refs. [6] and [7] show that Ps formed from MOF samples involves another new mechanism for the production of Ps in vacuum [19, 20]. We conclude that we have observed Ps emission from Bloch states in MOF crystals and identified the emission energies with features of the Ps interactions in these crystals. The narrow energy width of the lowest energy peak of ZIF-8, which accounts for as much as $\sim 10\%$ of the implanted positrons at $K = 2$ keV, allows for the prospect of efficiently decelerating or focusing the emitted Ps using Rydberg Ps electrostatic optics [21]. The Ps emission should be predominantly in a direction normal to the MOF crystal surfaces which are (100) for MOF-5 (*cf.* supplementary material of Ref. [6]) and (110) for ZIF-8 [22]. Thus a single MOF crystal should yield a narrow Ps beam with angular spread $\sqrt{k_B T/A}$. There should be other interesting possibilities for further study, given the fact that there are so many different members of the MOF family [23]. In particular, increasing the lattice constant, for example from the half-lattice constant 1.2915 nm of MOF-5 to 2.149 nm of MOF-16, could lead to a Ps state with very low emission energy and small energy spread that would be very useful for precision Ps 1S-2S spectroscopy [24] and for measurements of the gravitational acceleration of Ps [25] and antihydrogen [26, 27].

It would also be interesting to determine what positron implantation energy densities can be tolerated and to see what self-interactions emerge when large densities of Ps atoms are formed within a MOF crystal [28]. For example a swarm of Ps might become trapped in the local crystal deformation of its own making and proceed to form a Bose-Einstein condensate [29, 30]. Possible densities could be of order one Ps per unit cell, for which the BEC critical temperature, assuming a relative Ps effective mass $M^* \approx 2$, would be above room temperature. This possibility makes MOF targets a promising avenue for achieving a Ps BEC.

The authors would like to thank Dr. D. B. Cassidy for helpful comments in preparing the manuscript. The positron experiments were supported in part by the US National Science Foundation under grants PHY 1206100 and PHY 1040590. Q. Zhai and P. Feng were supported by DOE BES DE-FG02-13ER46972 (MOF-5 synthesis and characterization).

* Contact information: adric.jones@ucr.edu

[1] H. Li, M. Eddaoudi, M. O'Keeffe, and O. M. Yaghi, Nature **402**, 276 (1999).
[2] M. Deutsch, Phys. Rev. **82**, 455 (1951).
[3] S. Berko and H. N. Pendelton, Annu. Rev. Nucl. Part. Sci. **30**, 543 (1980).
[4] M. Charlton and J. W. Humberston, *Positron Physics* (Cambridge University Press, 2001) iSBN 0 521 41550 0.
[5] A. Greenberger, A. P. Mills, Jr., A. Thompson, and S. Berko, Phys. Lett. A **32**, 72 (1970).
[6] D. Dutta, J. I. Feldblyum, D. W. Gidley, J. Imirzian, M. Liu, A. J. Matzger, R. S. Vallery, and A. G. Wong-Foy, Phys. Rev. Lett. **110**, 197403 (2013).
[7] P. Crivelli, D. Cooke, B. Barbiellini, B. L. Brown, J. I. Feldblyum, P. Guo, D. W. Gidley, L. Gerchow, and A. J. Matzger, Phys. Rev. B **89**, 241103(R) (2014).
[8] A. C. L. Jones, T. H. Hisakado, H. J. Goldman, H. W. K. Tom, and A. P. Mills, Jr., (2015), in preparation.
[9] D. B. Cassidy, T. H. Hisakado, H. W. K. Tom, and A. P. Mills, Phys. Rev. Lett. **108**, 043401 (2012).
[10] A. P. Mills, Jr. and E. M. Gullikson, Applied Physics Letters **49**, 1121 (1986).
[11] R. G. Greaves and C. M. Surko, Nucl. Instrum. Meth. B **192**, 90 (2002).
[12] A. P. Mills, Jr., E. D. Shaw, R. J. Chichester, and D. M. Zuckerman, Phys. Rev. B **40**, 8616 (1989).
[13] The signal from the MCP is recorded on a digital oscilloscope (Agilent 54855A DSO) at a rate of 2 samples per ns with an 11 point sliding average applied. The times of MCP events are defined as the times when the

MCP voltage signal crosses a 2 mV threshold level, as determined by post-experiment analysis of the oscilloscope traces recorded after each positron pulse.
[14] P. Sferlazzo, S. Berko, and K. F. Canter, Phys. Rev. B **32**, 6067 (1985).
[15] D. W. Brown and Z. Ivić, Phys. Rev. B **40**, 9876 (1989).
[16] W. Y. Liang and A. D. Yoffe, Phys. Rev. Lett. **20**, 59 (1968).
[17] Y. Toyozawa and J. Hermanson, Phys. Rev. Lett. **21**, 1637 (1968).
[18] T. Hyodo, J.-I. Kasai, and Y. Takakusa, J. Phys. Soc. Japan **49**, 2248 (1980).
[19] D. B. Cassidy, T. H. Hisakado, H. W. K. Tom, and A. P. Mills, Jr., Phys. Rev. Lett. **106**, 133401 (2011).
[20] D. B. Cassidy, T. H. Hisakado, H. W. K. Tom, and A. P. Mills, Jr., Phys. Rev. Lett. **107**, 033401 (2011).
[21] D. B. Cassidy and S. D. Hogan, Int. J. Mod. Phys. Conf. Ser. **30**, 1460259 (2014).
[22] M. He, J. Yao, Q. Liu, K. Wang, F. Chen, and H. Wang, Micropor. Mesopor. Mat. **184**, 55 (2014).
[23] D. J. Tranchemontagne, L. José Mendoza-Cortés, M. O'Keeffe, and O. M. Yaghi, Chem. Soc. Rev. **38**, 1257 (2009).
[24] S. G. Karshenboim, Int. J. Mod. Phys. A **19**, 3879 (2004).
[25] A. P. Mills, Jr. and M. Leventhal, Nucl. Instrum. and Meth. B **192**, 102 (2002).
[26] A. Kellerbauer, *et al.*, Nucl. Instrum. Meth. B **266**, 351 (2008).
[27] P. Perez and Y. Sacquin, Classical Quant. Grav. **29**, 184008 (2012).
[28] D. B. Cassidy, S. H. M. Deng, R. G. Greaves, T. Maruo, N. Nishiyama, J. B. Snyder, H. K. M. Tanaka, and A. P. Mills, Jr., Phys. Rev. Lett. **95**, 195006 (2005).
[29] P. M. Platzman and A. P. Mills, Jr., Phys. Rev. B **49**, 454 (1994).
[30] Y.-H. Wang, B. M. Anderson, and C. W. Clark, Phys. Rev. A **89**, 043624 (2014).